Global and Planetary Change 207 (2021) 103675

Contents lists available at ScienceDirect

Global and Planetary Change

journal homepage: www.elsevier.com/locate/gloplacha

Research Paper

Coral perspective on temperature seasonality and interannual variability in the northern South China Sea during the Roman Warm Period

Leilei Jiang [a], Kefu Yu [a,b,*], Tao Han [c,a], Shichen Tao [d], Huiling Zhang [e]

[a] Guangxi Laboratory on the Study of Coral Reefs in the South China Sea, Coral Reef Research Centre of China, School of Marine Sciences, Guangxi University, Nanning 530004, China
[b] Southern Marine Sciences and Engineering Guangdong Laboratory (Zhuhai), Zhuhai 519082, China
[c] State Key Laboratory of Loess and Quaternary Geology, Institute of Earth Environment, Chinese Academy of Sciences, Xi'an 710061, China
[d] Key Laboratory of Ocean and Marginal Sea Geology, South China Sea Institute of Oceanology, Chinese Academy of Sciences, 510301 Guangzhou, China
[e] College of Ocean Engineering, Guangdong Ocean University, Zhanjiang 524088, China

ARTICLE INFO

Editor: Haywood Alan

Keywords:
Coral Sr/Ca
Sea-surface temperature
Seasonality
El Niño–Southern Oscillation
Roman Warm Period
South China Sea

ABSTRACT

Few reconstructions of sea-surface temperature (SST) have focused on seasonal and interannual variability, two major components of the global climate system, due to the limited temporal resolution of proxies. This study presents a combined 228-year-long, monthly resolved strontium to calcium ratios (Sr/Ca) record covering the period of 2070–1740 a BP (years before 1950 CE (Common Era)) extracted from three U-series-based sub-fossil *Porites* corals located on the Xisha Islands, northern South China Sea (SCS). The composite time series allowed for accurate assessment of the natural range of SST variations during snapshots of the Roman Warm Period (RWP). Reconstructed SST revealed that the RWP was characterized by cooler conditions compared with the 20th century, consistent with climatic variations in the western Pacific and East Asia. The amplitude of SST seasonality was within the modern range, except for a lower value at 1980–1928 a BP. Interannual variability associated with El Niño–Southern Oscillation (ENSO) activity was enhanced by 39% relative to 1980–2014 CE. The results of the sliding window demonstrate that ENSO variability persistently strengthened during 2070–2010 a BP, followed by an overall fluctuating attenuation during 1980–1928 a BP. Then, the trends of rising first before descending twice during 1852–1800 a BP appeared. Furthermore, ENSO activity played a leading role in steering short-term changes in SST seasonality in the northern SCS, manifested as stronger ENSO activity with more frequent El Niño events and decreased SST seasonality. Considering that the frequency of extreme ENSO events may strengthen in the future under global warming, the climate in the northern SCS might become more variable and complex.

1. Introduction

As the primary components and physical descriptors of climate systems, seasonality and interannual variability in sea-surface temperature (SST) have dramatic impacts on the Earth's surface system (Denton et al., 2005; Giry et al., 2012; Patterson et al., 2010; Yan et al., 2015a). However, the predictability of SST variation on these timescales remains challenging due in part to the incomplete understanding of its long-term changes and forcing mechanisms, which stem primarily from the insufficient length and spatial coverage of modern observations and reanalysis products for SST (Deser et al., 2010; Smith et al., 2008). Therefore, reconstructions of SST seasonality and interannual variability in the preindustrial era, especially over the last two millennia, are crucial for comprehensively understanding past climate change, assessing current climatic conditions, researching forcing mechanisms, and improving the accuracy of future climatic predictions (Dee et al., 2020; Deng et al., 2019; Ge et al., 2013).

The Roman Warm Period (RWP), also called the Roman Climate Optimum episode (Wang et al., 2012), covers the first centuries of the Common Era (CE) (2200–1550 a BP (years before 1950 CE); Steinke et al., 2014). It has been proposed as one of the most recent two natural warm periods in the last two millennia due to the general warmth in the North Atlantic and Europe (Büntgen et al., 2011; Lamb, 1977; Ljungqvist, 2010; Martín-Puertas et al., 2009). Reconstructions of high-resolution SST during the RWP provide an important benchmark for understanding the influence of external forcings and internal climate

* Corresponding author at: School of Marine Sciences, Guangxi University, No. 100, Daxuedong Road, Xixiangtang District, Nanning 530004, Guangxi, China.
E-mail address: kefuyu@scsio.ac.cn (K. Yu).

https://doi.org/10.1016/j.gloplacha.2021.103675
Received 17 May 2021; Received in revised form 30 September 2021; Accepted 4 October 2021
Available online 8 October 2021

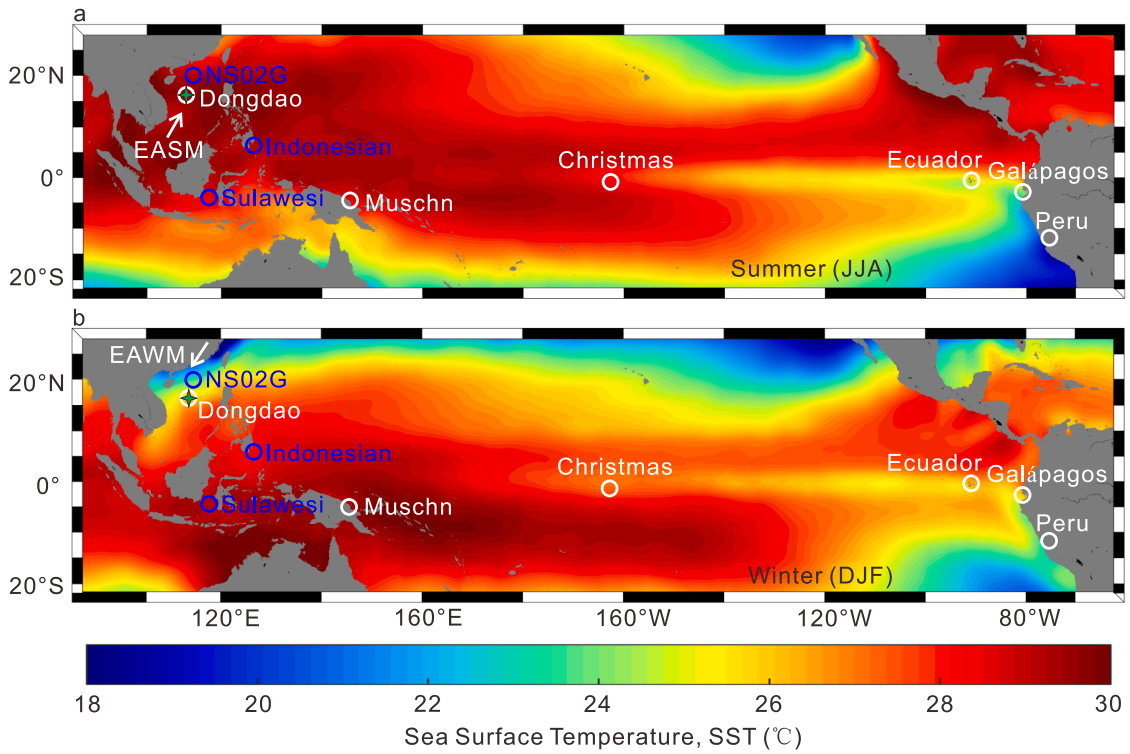

Fig. 1. Satellite-derived sea surface temperature (SST) across the tropical Pacific during strong El Niño events for 1980–2000 CE (Reynolds et al., 2002). (a) Average summer (June–July–August: JJA) SST with the direction of the East Asian summer monsoon (EASM). (b) Average winter (December–January–February: DJF) SST with the direction of the East Asian winter monsoon (EAWM). Blue circles indicate the locations of SST estimates from the northern South China Sea (NS02G: Kong et al., 2017), Sulawesi margin (Oppo et al., 2009), and Indonesian (Stott et al., 2004). White circles indicate the locations of ENSO reconstruction from Dongdao Island (Yan et al., 2017), Muschn Island (McGregor and Gagan, 2004), Christmas Island (Cobb et al., 2013; Woodroffe et al., 2003), Galápagos (Conroy et al., 2008; Koutavas et al., 2006; Riedinger et al., 2002), Ecuador (Moy et al., 2002), and Peru (Makou et al., 2010; Rein et al., 2005). Green stars indicate the location of coral samples from the Xisha Islands. (For interpretation of the references to colour in this figure legend, the reader is referred to the web version of this article.)

variability, distinguishing the relative contribution of natural processes and human actions to climate change, and predicting the likelihood of the occurrence of similar climate variations in the future (Wu et al., 2012). In recent decades, considerable progress has been made in the reconstruction of SST during the RWP (Oppo et al., 2009; Neukom et al., 2019; Wu et al., 2012). However, the temporal and spatial distribution of warm climatic conditions during this period remains controversial. Several paleoclimatic reconstructions indicate that relatively cold periods occurred 2000 years ago (Deng et al., 2019; Moberg et al., 2005). Additionally, an overwhelming majority of high-resolution paleoclimatic records that can quantify SST seasonality were obtained from high latitudes (Wanamaker Jr. et al., 2011; Wang et al., 2012). On interannual timescales, El Niño–Southern Oscillation (ENSO) variability during the RWP also exhibited large uncertainties (Cobb et al., 2013; Conroy et al., 2008; McGregor and Gagan, 2004; Steinke et al., 2014; Yan et al., 2017). These results indicate large gaps in SST variations of the tropical Pacific approximately 2000 years ago and emphasize the necessity of reconstructing additional monthly resolved SSTs.

Massive hermatypic corals are one of the excellent high-resolution paleoclimatic and paleoceanographic archives due to their rapid growth rate (up to 2 cm per year), long lifespan (centuries), and clear annual-density bands (Corrège, 2006; Yu, 2012). Among a remarkable array of geochemical tracers within the coral skeleton, strontium to calcium ratios (Sr/Ca) are a powerful tool for reconstructing past sea surface thermal variations because coral Sr/Ca varies primarily as a function of SST during their growth phases (Corrège, 2006; DeLong et al., 2014; Yu et al., 2005a). Precisely dated coral Sr/Ca time series have the ability to track changes in SST with monthly to annual resolution, allowing for continuous reconstruction of seasonal to multi-decadal SST variability that spans several centuries (Gagan et al., 1998; Jiang et al., 2021; Kong et al., 2017; Linsley et al., 2000; Yu et al., 2005b). Furthermore, coral Sr/Ca-SST records can perfectly compensate for deficiencies in the coarse resolution of marine sediment archives (Wu et al., 2012) and shorter lived bivalves (Wang et al., 2012; Yan et al., 2015a).

The South China Sea (SCS), one of the largest marginal seas in the western Pacific that contains abundant corals (Fig. 1), is an ideal area for studying multi-timescale SST variations (Mitsuguchi et al., 2008; Yu, 2012). Previous studies derived from *Tridacna gigas* have revealed SST seasonality and interannual variability in the northern SCS approximately 2000 years ago (Yan et al., 2015a; Yan et al., 2017). However, these records are insufficient to quantify SST variations over the whole RWP due to the short lifespan inherent in individual proxies. The relationship between seasonality and interannual variability has also not been revealed. In this study, a total of 228-year-long, monthly SST records were generated for snapshots of the RWP, with individual time windows of up to 113 years length, based on three spliced *Porites* coral Sr/Ca time series from the northern SCS. The main objective was to reveal the characteristics of SST variation on seasonal and interannual timescales, reconstruct past ENSO activity, and explore the relationship between SST seasonality and ENSO variability.

2. Modern climatic conditions

The SCS, an important bridge connecting high- and low-latitude climate processes, is of the most complex regions of the global climate system (Jiang et al., 2021; Mitsuguchi et al., 2008). The Xisha Islands are an archipelago located in the northwestern SCS (Fig. 1), where SST variations are dominated by the combined influence of ENSO and the East Asian monsoon (EAM). Seasonal climate variations are mainly

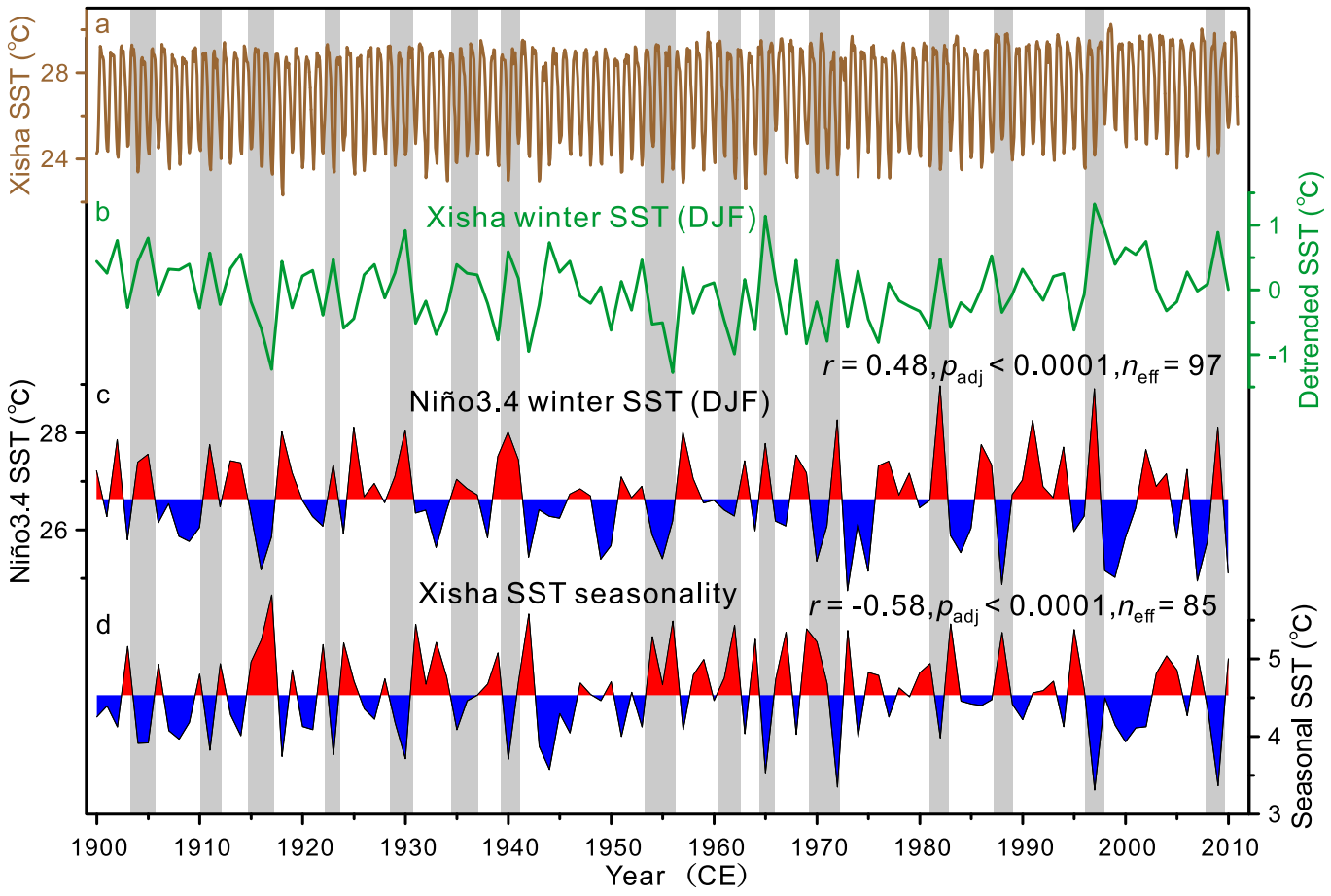

Fig. 2. Comparison of instrumental SST from the Xisha Islands with Niño3.4 SST during 1900–2010 CE. (a) Monthly SST time series, representative of a 1° × 1° grid centered on the Xisha Islands (16°N–17°N, 112°E–113°E) (Rayner et al., 2003). (b) Detrended winter (December–January–February: DJF) Xisha SST time series. (c) Winter Niño3.4 SST time series. (d) Xisha SST seasonality calculated as the difference between summer (June–July–August: JJA) and winter SST in a single year. Among them, winter Niño3.4 SST was significantly correlated with the detrended winter Xisha SST ($r = 0.48$, $p_{adj} < 0.0001$, $n_{eff} = 97$) and Xisha SST seasonality ($r = -0.58$, $p_{adj} < 0.0001$, $n_{eff} = 85$). Gray vertical fields indicate the major El Niño events or La Niña events that were followed by anomalous SST seasonality around the Xisha Islands.

controlled by EAM, characterized by warm southwest winds in boreal summer (June–July–August: JJA) and cold northeast winds in boreal winter (December–January–February: DJF) (Wyrtki, 1961). Instrumental SST from the Xisha Islands suggests a mean summer SST of 29.2 ± 0.4 (1σ) °C and a mean winter SST of 24.7 ± 0.6 (1σ) °C, resulting in a mean seasonal SST of 4.5 ± 0.6 (1σ) °C for 1960–2016 CE (Rayner et al., 2003; Fig. S1). On interannual timescales, SST in the northern SCS was remotely modulated by ENSO activity (Jiang et al., 2021; Wang et al., 2000). For example, a strong El Niño event in 1997 CE generated an anomalous warm SST in the northern SCS, which was recorded by coral skeletons (Wang et al., 2018). In addition, there are complicated interactions between ENSO activity and EAM circulations (Mitsuguchi et al., 2008; Wang et al., 2000).

Modern observations have shown that El Niño events usually emerge in boreal spring (March–April–May: MAM), grow during boreal summer and autumn (September–October–November: SON), reach their maximum intensity in boreal winter, and decay rapidly during late winter and next spring (McGregor et al., 2013; Timmermann et al., 2018). Mature phases of ENSO that generally occur in boreal winter have remotely affected SST in the northern SCS (Klein et al., 1999). Therefore, there was a significant correlation between the Niño3.4 index (DJF) and the detrended winter Xisha SST for 1900–2010 CE ($r = 0.48$, $p_{adj} < 0.0001$, $n_{eff} = 97$; Fig. 2). Considering that ENSO primarily affects Xisha SST anomalies in winter (the coldest season), it is obvious that the remote influence of ENSO affects Xisha SST seasonality. The Niño3.4 index (DJF) is negatively correlated with the amplitude of SST seasonality (the difference between summer and winter SST) in the Xisha Islands ($r = -0.58$, $p_{adj} < 0.0001$, $n_{eff} = 85$; Fig. 2), suggesting that El Niño events contribute to decreased amplitude and La Niña events lead to increased SST seasonality amplitude. In summer, SST in the northern SCS is mainly governed by the Western Pacific Warm Pool moving northward (Yan et al., 2015a). There was no conspicuous difference in Xisha summer SST among the different phases of ENSO activity (Fig. S2). In winter, El Niño events are conducive to the formation of the anomalous anticyclone over the western North Pacific, weakening the East Asian winter monsoon (EAWM), and yield positive SST anomalies in the northern SCS (Li, 1990; Wang et al., 2000). Conversely, La Niña events contribute to strong northeast winds that reduce winter SST in the Xisha Islands. Therefore, the amplitude of SST seasonality in the Xisha Islands during El Niño events tends to be weaker than that of La Niña events (Fig. S2).

3. Materials and methods

3.1. Coral collection and pretreatment

Three in situ sub-fossil *Porites lutea* coral cores recovered from two atolls in the Xisha Islands are presented (Fig. S3). During the field work in 2008 CE, sample GQD4 was drilled at an ~5 m water depth off Ganquan Island (16°30′28″N, 111°35′10″E) along the primary vertical

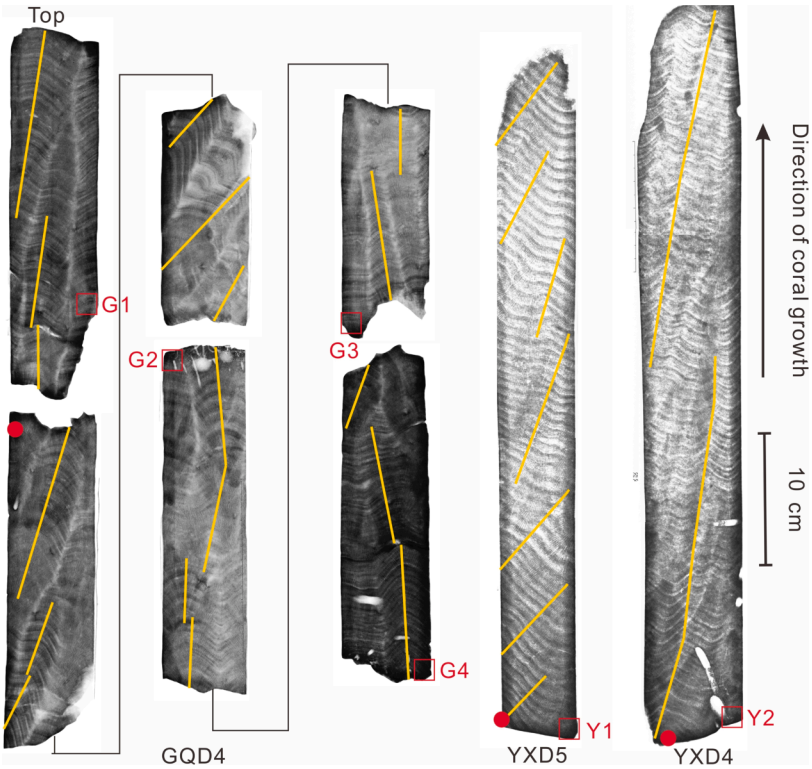

Fig. 3. X-radiograph positive images of sub-fossil *Porites lutea* coral core slabs for GQD4, YXD5, and YXD4. X-rays show clear annual banding made up of low-density and high-density bands. Yellow lines indicate the sub-sampling transects along the maximum growth axis. Red rectangles indicate the location of thin sections that were used to assess the preservation of coral aragonite. Red points denote the location of samples selected for high-precision TIMS U-series dating. (For interpretation of the references to colour in this figure legend, the reader is referred to the web version of this article.)

growth axis. Samples YXD4 and YXD5 were retrieved from two massive corals offshore Yongxing Island (16°50′30″N, 112°19′48″E and 16°50′35″N, 112°19′52″E). Modern sample YXN1, previously used to calibrate the coral Sr/Ca-SST relationship in the northern SCS, was obtained from living *P. lutea* coral off Yongxing Island (Jiang et al., 2021). Another modern coral 15XS1 presented by Wang et al. (2018) was

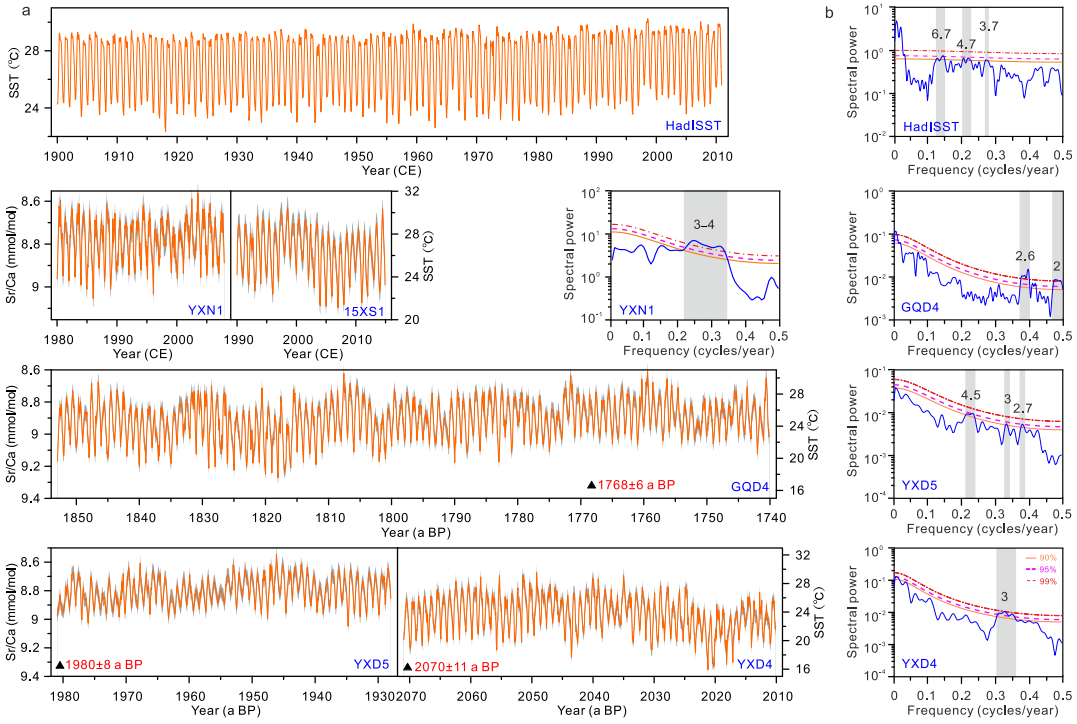

Fig. 4. Time series of SST records and their spectral properties. (a) Instrumental SST (Rayner et al., 2003) and monthly coral Sr/Ca records from the Xisha Islands. Sr/Ca axes were reversed so that warmer values (i.e., lower Sr/Ca values) are up. Reconstructed SST (orange line) with Monte Carlo uncertainty quantification (gray shading) was calculated using the published method described by Jiang et al. (2021). Black triangles mark the ^{230}Th ages for individual sub-fossil corals. (b) Multitaper method (MTM) spectral analysis with the red noise null hypothesis (number of tapers, 3; bandwidth parameter, 2) for the detrended and normalized SST records (Ghil et al., 2002). The significant periodicities (year) above the 90% confidence level (orange line) are indicated by gray vertical fields. (For interpretation of the references to colour in this figure legend, the reader is referred to the web version of this article.)

collected from Qilianyu Reef in September 2015. Details of coral samples are displayed in Table S1.

Coral cores were vertically sliced into approximately 7-mm thick slabs along the growth directions. Slabs were kept in 5% H_2O_2 for 48 h to decompose organic matter, rinsed three times with deionized water in an ultrasonic water bath for 5–10 min each time, and then dried in a 60 °C oven. Finally, X-radiograph images of individual coral slabs were taken by a medical X-ray machine to distinguish the annual-density bands and determine the maximum growth axis for microsampling (Fig. 3). The growth rate of three sub-fossil corals, which is the distance between high- and low-density band couplets, ranged from 9 to 12 mm/year (Table S1). Furthermore, small blocks extracted from sub-fossil corals were examined for possible diagenetic alteration (Fig. 3). The results of X-ray diffraction (Fig. S4) and scanning electron microscopy (Fig. S5) revealed the absence of secondary aragonite or calcite cements and excellent preservation of the original skeletal microstructure.

3.2. Geochemical analyses

Coral samples for Sr/Ca analyses were collected from the surface of each slab along the maximum growth axis of the corallite fan using a digitally controlled milling machine (DeLong et al., 2013 and therein) (Fig. 3). Coral powder was extracted in succession by milling at ~0.8-mm increments, which yielded a resolution of approximately 12 samples per year. Approximately 1.0 mg of coral powder was fully dissolved in 2% HNO_3 to obtain a final Ca concentration of ~40 ppm. Coral Sr/Ca solutions were analyzed on a Varian Vista Pro (Varian Inc., U.S.A.) inductively coupled plasma atomic emission spectroscope at Guangxi University, following previous techniques (Jiang et al., 2021; Schrag, 1999; Yu et al., 2005b). The in-house standard (NS-1), homogenized powder extracted from a *P. lutea* coral, was measured after every two coral samples and applied to the raw coral Sr/Ca data to correct for linear drift. The analytical precision was 0.016 mmol/mol (1σ; n = 1984), yielding an uncertainty of ~0.3 °C according to the coral Sr/Ca thermometer from the Xisha Islands (−0.0497 mmol/mol per 1 °C, Jiang et al., 2021). Moreover, the international coral standard (JCp-1; Okai et al., 2002) was also measured and determined a mean Sr/Ca value of 8.647 ± 0.069 (2σ) mmol/mol (n = 225), which was within the analytical error of the mean value of 8.838 ± 0.089 (2σ) mmol/mol reported in Hathorne et al. (2013).

3.3. Chronology

Uranium-thorium (U-Th) isotopic measurements were undertaken at the Radiogenic Isotope Facility of the University of Queensland by a Nu plasma high-resolution multicollector inductively coupled plasma mass spectrometer following the method described by Yu et al. (2006). Approximately 1 g of coral fragments was spiked with a ^{229}Th–^{233}U–^{236}U mixed tracer and dissolved in double-distilled nitric acid to conduct chemical treatment and mass spectrometry (Yu et al., 2012). Coral GQD4, YXD5, and YXD4 were dated at 1768 ± 6 (2σ) a BP, 1980 ± 8 (2σ) a BP, and 2070 ± 11 (2σ) a BP, respectively (Table S2). This shows sub-fossil corals lived during the RWP (Steinke et al., 2014).

The chronology of sub-fossil corals was determined by a combination of U-series dating, annual-density bands, and annual cycles of Sr/Ca records (Fig. 4a). According to the obvious annual cycle of instrumental SST from the Xisha Islands for 1900–2010 CE (Rayner et al., 2003), the highest (lowest) coral Sr/Ca was assigned to January (June) in any given year, corresponding to the peak of boreal winter (summer) SST (Fig. S1). The measured coral Sr/Ca data were converted from depth series into time series with monthly resolution (12 equidistant points per year) by performing linear interpolation between these anchor points. Ultimately, coral GQD4, YXD5, and YXD4 were identified to cover the periods of 1852–1740 a BP, 1980–1928 a BP, and 2070–2010 a BP, respectively.

3.4. Statistics analyses

Coral Sr/Ca records were translated into SST estimates based on the monthly relationship of −0.0497 mmol/mol per 1 °C (Jiang et al., 2021). To address the uncertainties associated with coral Sr/Ca-SST estimates, we applied the combined error determined by Monte Carlo simulations of 1000 synthetic datasets that take analytical uncertainty, intercolony uncertainty, and calibration uncertainty into account

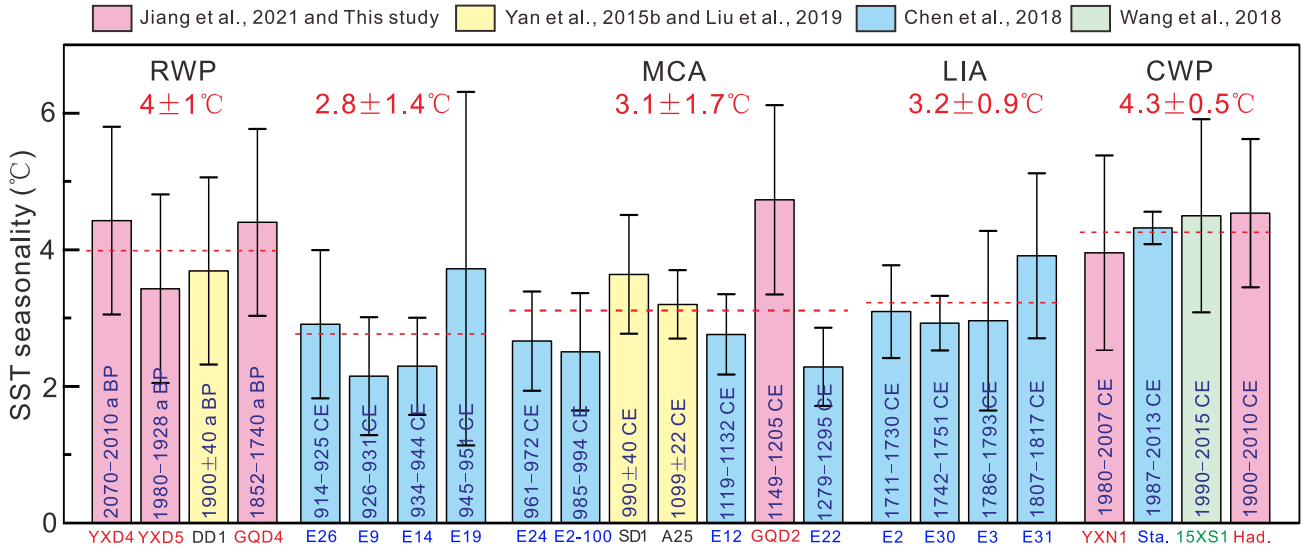

Fig. 5. Comparison of Sr/Ca-derived SST seasonality (the difference between summer and winter SST) calculated from individual corals (Chen et al., 2018; Jiang et al., 2021; Wang et al., 2018), *Tridacna* shell (Liu et al., 2019; Yan et al., 2015b), and instrumental SST (Rayner et al., 2003) from the Xisha Islands. The horizontal red dashed line represents the mean Sr/Ca-SST seasonality calculated from the mean seasonality of corals during the different periods (RWP, Roman Warm Period; MCA, Medieval Climate Anomaly; LIA, Little Ice Age; CWP, Current Warm Period). Error bars for sub-fossil corals represent the combined error (root of the sum of the squares) of the standard deviation (2σ) of the mean Sr/Ca seasonality of modern *Porites* spp. and the standard error (2SE) of the averaged Sr/Ca seasonality of the sub-fossil coral, following established procedures (Abram et al., 2009) but applied to reconstructed seasonality from Chen et al. (2018) and this study. 2SE for modern corals and instrumental data were presented. (For interpretation of the references to colour in this figure legend, the reader is referred to the web version of this article.)

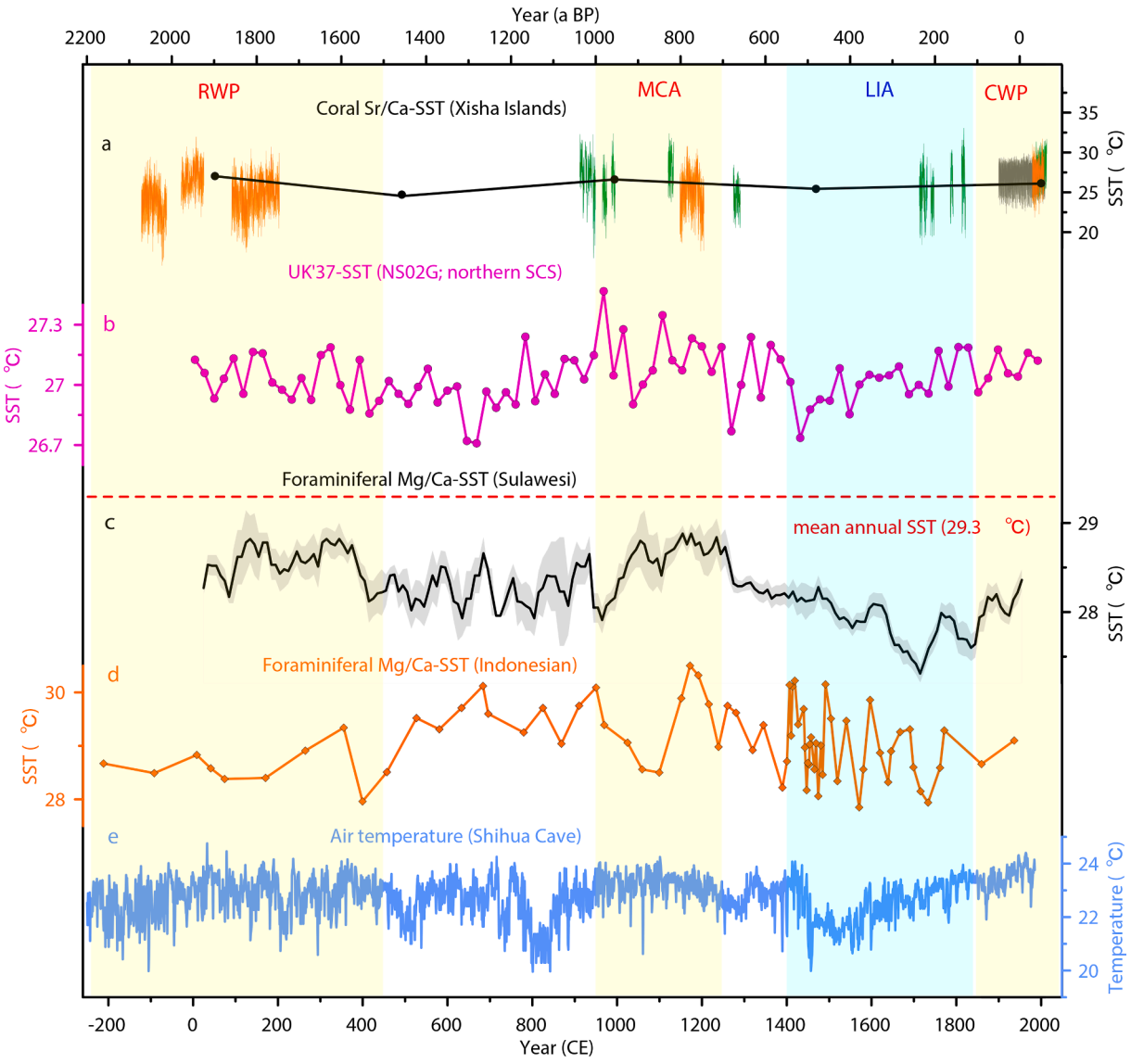

Fig. 6. Comparison of temperature reconstructions around the western Pacific during the last 2000 years. (a) Instrumental SST (gray line: Rayner et al., 2003) and coral Sr/Ca-SST estimates (green lines: Chen et al., 2018; black line: Yan et al., 2015a; orange lines: Jiang et al., 2021 and this study) from the Xisha Islands. (b) SST records based on the long-chain alkenones Uk'37 from the northern SCS (Kong et al., 2017). (c) Composite foraminiferal Mg/Ca-SST records and mean annual SST for 1997–2007 CE (horizontal red dashed line) from the Sulawesi margin (Oppo et al., 2009). (d) Foraminiferal Mg/Ca-SST estimates from Indonesia (Stott et al., 2004). (e) Air temperature estimates from Shihua Cave in Beijing (Tan et al., 2003). Yellow and blue vertical fields indicate the approximate intervals for the warm (RWP, Roman Warm Period; MCA, Medieval Climate Anomaly; CWP, Current Warm Period) and cold periods (LIA, Little Ice Age), respectively. (For interpretation of the references to colour in this figure legend, the reader is referred to the web version of this article.)

according to established procedures (Jiang et al., 2021). Mean SST was calculated by averaging monthly data of each year and then averaging the resulting annual means of the whole period. SST seasonality was defined as the difference between summer and winter SST in a given year, corresponding to the warmest and coldest seasons. Mean SST seasonality was calculated by averaging the resulting SST seasonality of the whole period. To fully account for the uncertainties related to mean Sr/Ca-SST estimates from individual sub-fossil *Porites* coral, the combined error (root of the sum of the squares) of the standard deviation (2σ) of mean Sr/Ca-SST of the two modern corals and the standard error (2SE) of mean Sr/Ca records for each sub-fossil coral were applied (Abram et al., 2009). The error assigned to the mean Sr/Ca-SST seasonality for each sub-fossil coral also follows a similar combination (Giry et al., 2012). Student's *t*-test was used to determine whether there was a significant difference between the mean values of two datasets (mean SST in Section 4.1 or mean SST seasonality in Section 4.2). The effective degrees of freedom (n_{eff}) were considered when we conducted significance tests (p_{adj}) for correlation analysis (Box et al., 1976; Jiang et al., 2021).

ENSO activity was tracked in continuous coral Sr/Ca-SST records by the interannual bands of multitaper method (MTM) spectral analysis (Ghil et al., 2002; Fig. 4b). To extract the ENSO component of SST variations, a 3–7-year band-pass filter was applied to monthly SST anomalies calculated by subtracting the averaged annual cycle from the monthly SST series (Fig. 8a). The total variance of filtered SST anomalies was used to evaluate the overall intensity of ENSO activity (McGregor et al., 2013; Jiang et al., 2021). An empirically calibrated threshold was applied to the filtered SST anomalies to investigate the frequency of ENSO events (Cobb et al., 2003; Jiang et al., 2021). Furthermore, the relative ENSO variance during the RWP using a sliding 31-year window was determined to assess changes in the strength of ENSO variability relative to the period of 1980–2007 CE (Cobb et al., 2013; D'Arrigo

et al., 2005; Jiang et al., 2021; Fig. 8c).

4. Results

4.1. Mean SST variations

All monthly coral Sr/Ca records exhibit clear annual cycles with a total time window of 228 years (Fig. 4a). The annual average coral Sr/Ca ranged from 8.562 to 9.051 mmol/mol for 1980–2007 CE, from 8.631 to 9.094 mmol/mol for 1990–2014 CE, from 8.676 to 9.352 mmol/mol for 2070–2010 a BP, from 8.550 to 9.049 mmol/mol for 1980–1928 a BP, and from 8.614 to 9.271 mmol/mol for 1852–1740 a BP (Fig. 4a). Considering the combined error of mean Sr/Ca-SST estimates from sub-fossil corals, the mean SST for 2070–2010 a BP and 1852–1740 a BP was significantly lower than that of the present day ($p < 0.05$). However, the mean SST for 1980–1928 a BP agrees with the instrumental value within the range of error (Table S1). The results suggest that the mean SST in the Xisha Islands during the RWP was lower than that during modern times.

4.2. SST seasonality

Modern coral Sr/Ca records indicate a mean SST seasonality of 4 ± 1.4 (2SE) °C for 1980–2007 CE and 4.5 ± 1.4 (2SE) °C for 1990–2014 CE (Fig. 5), satisfactorily documenting instrumental SST seasonality of 4.5 ± 1.1 (2σ) °C for 1900–2010 CE (Rayner et al., 2003). There was no statistically significant difference between the two modern coral Sr/Ca-SST seasonalities ($p = 0.1$). Sub-fossil coral Sr/Ca records demonstrate a mean SST seasonality of 4.4 ± 1.4 (2SE) °C for 2070–2010 a BP and for 1852–1740 a BP, which was not significantly different from the modern value ($p > 0.05$) (Fig. 5). However, the mean SST seasonality of 1980–1928 a BP (3.4 ± 1.4 (2SE) °C) was significantly lower than that under modern conditions ($p \leq 0.05$) (Fig. 5). In summary, the RWP had similar SST seasonality to the 20th century, except for a relatively low value in 1980–1928 a BP. Additionally, the most striking result was that spectral analyses of SST seasonality reveal significant interannual variability for all time intervals (Fig. S6).

4.3. Interannual SST variability

Instrumental SST from the Xisha Islands was characterized by prominent interannual variability during 1900–2010 CE, with significant periodicities of 3–7 years (Fig. 4b). Spectral analyses of modern coral Sr/Ca-SST records indicated similar interannual variability. Pronounced interannual peaks ranging from two to five years were also identified in all sub-fossil coral Sr/Ca-SST records. It is noteworthy that the SST in 1980–1928 a BP displays a remarkable periodicity of 4.5 years, which was unprecedented in all other records (Fig. 4b). This means that interannual SST variability was stronger in this time interval than that in modern times and other periods of the RWP. The results of the total variance show that the ENSO intensity recorded by sub-fossil corals in 2070–2010 a BP (0.25 °C^2) and 1980–1928 a BP (0.31 °C^2) was obviously higher than that recorded by modern corals in 1980–2007 CE (0.19 °C^2) and 1990–2014 CE (0.17 °C^2). However, the ENSO intensity in 1852–1740 a BP (0.18 °C^2) was consistent with the modern intensity (Fig. S7). Therefore, ENSO activity during the RWP was considered to be stronger than that at present and reached its highest intensity in 1980–1928 a BP.

5. Discussion

5.1. Cooler than present SST during the RWP

It remains controversial whether SST from the tropical Pacific during the RWP exceeds modern conditions, due in part to the limited temporal resolution and lifespan of proxies (Deng et al., 2019; Neukom et al., 2019; Yan et al., 2015b). Coral Sr/Ca records provide a unique perspective for monthly SST reconstructions. However, intercolony offsets among *Porites* spp. corals can produce large uncertainties in Sr/Ca-derived SST estimates and present a significant obstacle to the reconstruction of absolute mean SST from individual fossil coral specimens (Abram et al., 2009; Cohen et al., 2002; DeLong et al., 2011; de Villiers et al., 1995; Felis et al., 2004; Linsley et al., 2006). The standard deviation (2σ) of the offsets in replicated modern coral Sr/Ca records from the Xisha Islands was 0.048 mmol/mol (Chen et al., 2018), which is equivalent to ~1 °C based on the local Sr/Ca-SST relationship (Jiang et al., 2021). Replicating coral Sr/Ca records across multiple overlapping specimens over a given time period can potentially minimize the uncertainties related to intercolony variability (Sayani et al., 2019). Therefore, a more rigorous calculation of the error is needed when using individual corals to reconstruct the mean SST.

Although intercolony offsets in mean Sr/Ca obstruct accurate quantification of mean SST, the result of cooler conditions during 2070–1740 a BP compared with the period of 1980–2014 CE was consistent with mean SST estimates based on coral growth rates from the Xisha Islands during the RWP (Huang et al., 2013). Similar conditions cooler than instrumental SST in the 20th century (27.1 ± 0.7 (2σ) °C for 1900–2010 CE) also appear to have existed here for the Medieval Climate Anomaly (MCA: 950–1250 CE) (Jiang et al., 2021), which was in agreement with multiple coral Sr/Ca-SST reconstructions from the Xisha Islands (Chen et al., 2018; Fig. 6a). Moreover, coral Sr/Ca records demonstrated that the SST in the Xisha Islands was cooler during the Little Ice Age (LIA: ~1400–1850 CE) than either the MCA or modern times (Chen et al., 2018). This means that SST warming in the 20th century was likely unprecedented in the northern SCS over the last 2000 years, which was inconsistent with the composite record of *Tridacna gigas* (Yan et al., 2015a). However, the alkenone-based SST record from the northern SCS suggests that the mean SST during the RWP was lower than that of the Current Warm Period (CWP: ~1850 CE to present) (Kong et al., 2017; Fig. 6b). Foraminiferal Mg/Ca records retrieved from sediment cores from the Sulawesi margin (Oppo et al., 2009; Fig. 6c) and the western Pacific (Stott et al., 2004; Fig. 6d) also illustrate that the SST approximately 2000 years ago did not exceed the mean SST of the CWP.

Furthermore, reconstructions of temperature in East Asia have broadly similar cold characteristics during the RWP. According to evidence recorded in Chinese historical documents, relatively cold phases existed from the Eastern Han Dynasty to the Three Kingdoms (1925–1670 a BP) (Chu, 1973). The poor harvests occurred in 2000–1360 a BP, further confirming the coldness of this period (Su et al., 2014). In particular, the climate experienced a cooling trend of −1.2 °C per century from 2040 a BP to 1920 a BP (Ge et al., 2013). Stalagmite $\delta^{18}O$ records from Shihua Cave in Beijing suggest that the air temperature of 2070–1922 a BP was ~0.9 °C lower than that of 1961–1980 CE (Tan et al., 2003; Fig. 6e), which was supported by pollen records in central Taiwan (Wang et al., 2019) and a multiproxy series in the Northern Hemisphere (Moberg et al., 2005). Although there were differences in the amplitudes and durations of temperature variations due to the different sampling sites and temporal resolutions, monthly coral Sr/Ca records from the Xisha Islands provide additional evidence for cooler conditions in the western Pacific and East Asia during the RWP.

5.2. Similar to present SST seasonality in 2070–1740 a BP

Few studies that have revealed historical SST seasonality using high-resolution proxies have concentrated on either the last millennium (Chen et al., 2018; Liu et al., 2019) or the Atlantic (Surge and Barrett, 2012; Wanamaker Jr. et al., 2011; Wang et al., 2012). The current study based on monthly coral Sr/Ca-SST records allows for addressing SST seasonality in the northern SCS for snapshots of 2070–1740 a BP. The results suggest that SST seasonality in 2070–2010 a BP and 1852–1740 a BP was similar to the present-day conditions, while a lower value was present in 1980–1928 a BP (Fig. 5).

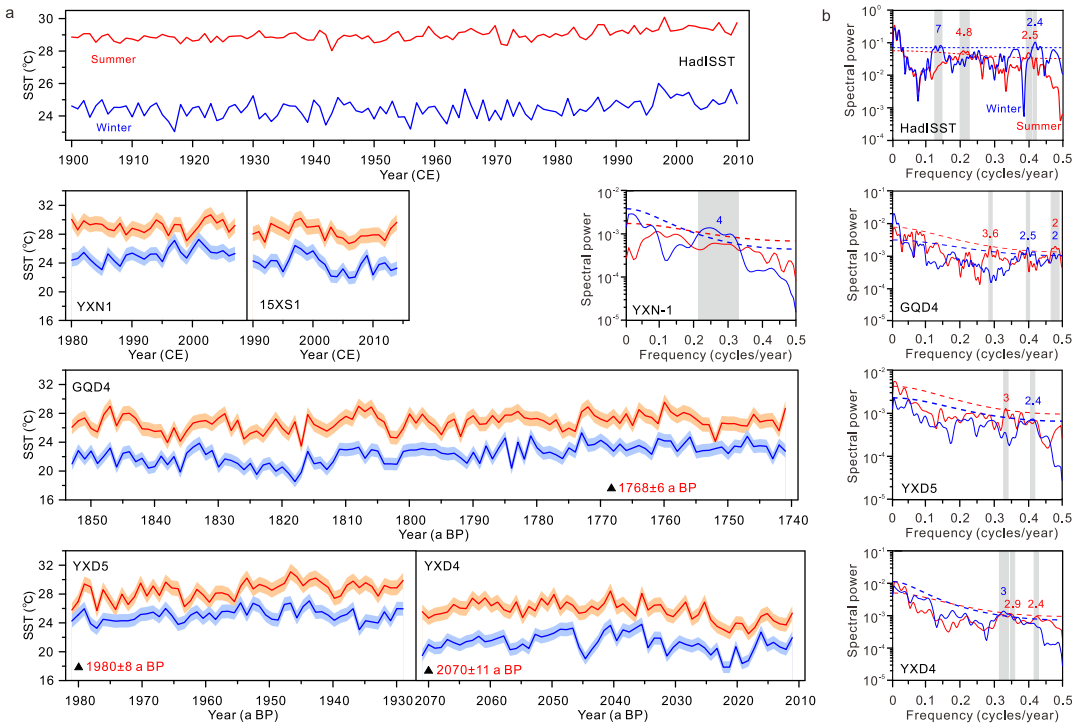

Fig. 7. Time series of summer and winter SST and their spectral properties. (a) Summer (June–July–August: JJA, red lines) and winter (December–January–February: DJF, blue lines) instrumental SST and coral Sr/Ca-SST records with Monte Carlo uncertainty quantification (light shading). Black triangles mark the ^{230}Th ages for individual sub-fossil corals. (b) Multitaper method (MTM) spectral estimates with a red noise null hypothesis (number of tapers, 3; bandwidth parameter, 2) for the detrended and normalized summer (red lines) and winter (blue lines) SST anomalies (Ghil et al., 2002). Numbers indicate significant periodicities (years) above the 90% confidence level (dashed lines). (For interpretation of the references to colour in this figure legend, the reader is referred to the web version of this article.)

SST variations in winter and summer were compared throughout this time interval (Fig. 7). Summer SST and winter SST for 2070–2010 a BP were 25.6 ± 1 (2SE) °C and 21.2 ± 0.9 (2SE) °C, respectively, which was ~3 °C lower than those recorded by modern corals (28.7 ± 1 (2SE) °C in summer and 24.5 ± 1 (2SE) °C in winter) and instrumental SST for 1900–2010 CE (29 ± 0.7 (2σ) °C in summer and 24.5 ± 1.1 (2σ) °C in winter). Similarly, summer SST and winter SST for 1852–1740 a BP are 26.8 ± 1 (2SE) °C and 22.4 ± 0.9 (2SE) °C, respectively, which was ~2 °C lower than those in the 20th century. Therefore, SST seasonality in the above two periods does not change significantly in comparison to the present. However, summer SST for 1980–1928 a BP (28.5 ± 1 (2SE) °C) was 0.2 °C lower than that exhibited by modern records, while winter SST of 25.1 ± 1 (2SE) °C was 0.6 °C warmer than that at present. Therefore, the SST seasonality for 1980–1928 a BP was obviously lower than the modern value. This was in accordance with the results derived from 48-year-long Sr/Ca ratios of *Tridacna gigas* from the Xisha Islands, which indicated that SST seasonality at approximately 1900 ± 40 a BP (3.69 ± 1.37 °C) was dramatically lower than that in recent decades (4.4 ± 0.82 °C for 1994–2005 CE) (Yan et al., 2015b; Fig. 5).

Previous studies have shown that the mean SST plays, to some extent, a prominent role in modulating SST seasonality in the northern SCS during the late Holocene (Yan et al., 2015a). When the background SST decreases, larger decrements in winter SST relative to summer SST cause increased SST seasonality. The opposite phenomenon takes place during the period of warmer mean SST. However, there was no obvious inverse relationship between the observed SST seasonality and mean SST throughout the RWP. For example, the lower SST seasonality but the similar mean SST to present occurred in the period of 1980–1928 a BP. Additionally, SST seasonality during the LIA was consistent with that of the MCA, which were lower than either the RWP or the CWP (Fig. 5). This can potentially signify that additional forcing mechanisms were critical in controlling variations in SST seasonality in the northern SCS.

5.3. Stronger than present ENSO activity in 2070–1740 a BP

ENSO, the dominant source of interannual climate variability, plays an important role in regulating temperature and rainfall patterns globally (Bjerknes, 1969; Jiang et al., 2021). Knowledge of past ENSO activity provides a crucial perspective for inferring the natural ENSO variability and its relation to climate forcing (Cobb et al., 2013; Lawman et al., 2020). However, the known ENSO reconstructions were mainly concentrated on the last millennium (Cobb et al., 2003; Dee et al., 2020; Li et al., 2011; Liu et al., 2019). In this study, the total variance of SST recorded by all sub-fossil corals (0.25 °C^2) was similar to that of the MCA (0.28 °C^2; Jiang et al., 2021) but larger than that recorded by modern corals (0.18 °C^2), indicating that ENSO activity during 2070–1740 a BP was enhanced by 39% compared with present day (Fig. S7).

Our finding of stronger ENSO activity during the RWP was broadly supported by a variety of late-Holocene paleoclimatic archives from the tropical Pacific. Laminated sediments from Bainbridge Crater Lake in the Galápagos Islands suggest an extremely high frequency of ENSO events in 2000–1750 a BP (Riedinger et al., 2002; Thompson et al., 2017), as indicated by the increase in lithic concentrations observed in sedimentation off the coast of Peru (Rein et al., 2005; Fig. 9b). Moreover, lake sediment records from Laguna Pallcacocha in southern Ecuador (Moy et al., 2002; Fig. 9c) and from El Junco in the Galápagos Islands (Conroy et al., 2008; Fig. 9d) reveal that maximum Holocene precipitation occurred between 2000 ± 100 a BP and 1500 ± 70 a BP, reflecting the peak amplitude of ENSO activity and the enhanced ENSO variability throughout this time interval. Such scenarios were further corroborated by individual foraminiferal δ^{18}O records from sediments near the Galápagos Islands, suggesting that SST in the ENSO source area increases drastically approximately 2000 a BP (Koutavas et al., 2006). Although the timing of ENSO variation inferred from individual records varies due to the different temporal resolutions, these records provide a reliable picture of stronger ENSO activity during the RWP.

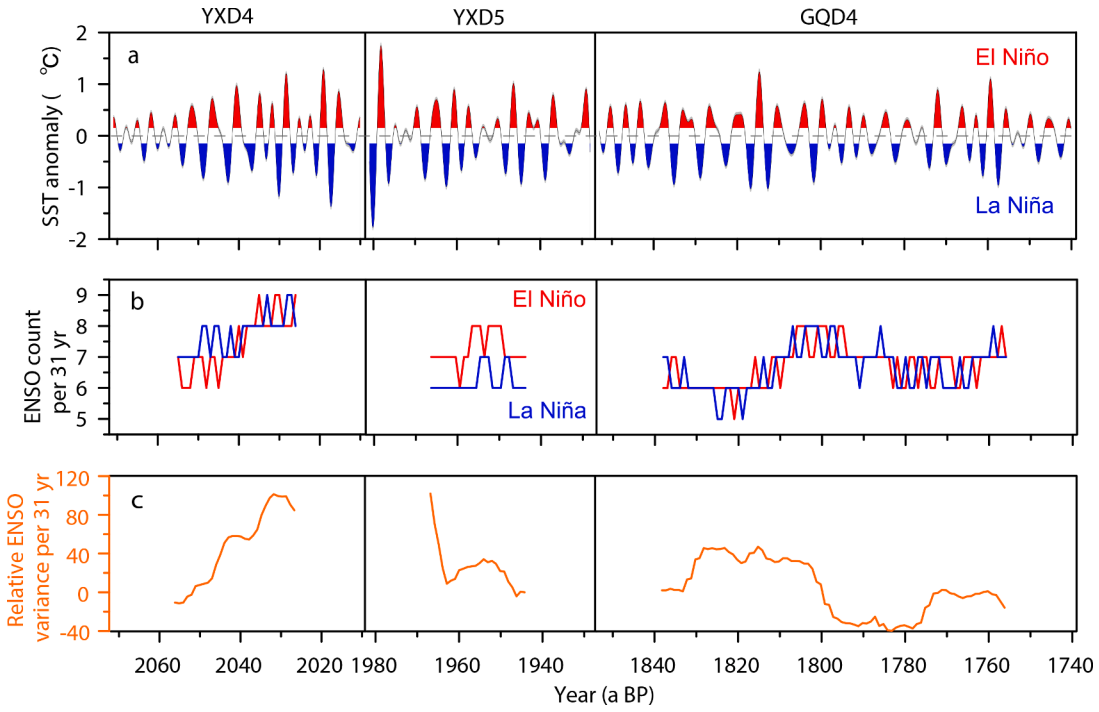

Fig. 8. ENSO reconstructions based on coral Sr/Ca records from the Xisha Islands during the Roman Warm Period. (a) 3–7-year band-pass filtered Xisha coral Sr/Ca-SST anomalies (black lines) with uncertainty quantification (gray shading). Red and blue shading indicate El Niño and La Niña events, respectively, defined by the asymmetric ENSO threshold (Jiang et al., 2021). (b) The number of El Niño (red line) and La Niña (blue line) events in ENSO chronologies using a sliding 31-year window. (c) Relative ENSO variance for the filtered sub-fossil coral Sr/Ca-SST anomalies in a sliding 31-year window, plotted as percent differences from the intervals of modern coral (1980–2007 CE). (For interpretation of the references to colour in this figure legend, the reader is referred to the web version of this article.)

In addition, the results of spectral analysis and total variance show that ENSO intensity varies substantially during the RWP. For example, ENSO activity in 1980–1928 a BP was obviously stronger than that in modern times, while ENSO intensity in 1852–1740 a BP was similar to that at present. Therefore, it was speculated that ENSO activity may have undergone significant changes during the RWP, which was not confirmed due to the dearth of long-term and high-resolution paleoclimatic records.

5.4. *Highly variable ENSO variability during the RWP*

The present study allowed for the verification of the hypothesis about the evolution of ENSO activity throughout the RWP. The asymmetric ENSO threshold identified by instrumental SST anomalies from the Xisha Islands, 0.15 °C for El Niño events and − 0.15 °C for La Niña events (Jiang et al., 2021), were applied to the filtered coral Sr/Ca-SST anomalies. The results indicate that 14 El Niño events and 15 La Niña events were estimated to have occurred during 2070–2010 a BP (Fig. 8a). The sliding window suggests a gradually increased frequency of ENSO events throughout this time (Fig. 8b). Meanwhile, the relative ENSO variance doubled from a level similar to modern times (Fig. 8c). A 19-year-long coral record from Muschn Island revealed protracted $\delta^{18}O$ anomalies indicative of a severe 7-year El Niño event approximately 2040 ± 50 a BP (McGregor and Gagan, 2004), which was in agreement with our coral records from the Xisha Islands. In addition, it is noteworthy that the variation in the frequency of El Niño events was larger than that of La Niña events, reflecting that El Niño events play a leading role in the evolution of ENSO variability (Fig. 8b).

A total of 12 El Niño events and 10 La Niña events were identified from 1980 a BP to 1928 a BP (Fig. 8a), which was almost consistent with a 50-year-long, monthly resolved *Tridacna gigas* $\delta^{18}O$ record from Dongdao Island, indicating 11 El Niño events and 12 La Niña events approximately 1900 ± 40 a BP (Yan et al., 2017). The sliding window shows that the frequency of El Niño events was always larger than that of La Niña events throughout this period (Fig. 8b). An approximately 90% reduction in relative ENSO variance was observed from 1980 a BP to 1960 a BP, while the lowest ENSO variance during this period was still 10% above current levels. In the following 30 years, the relative ENSO variance slowly increased by 20% and then dropped to the level equivalent to modern times (Fig. 8c).

Twenty-four El Niño events and 24 La Niña events were observed from 1852 a BP to 1740 a BP (Fig. 8a). In the first 20 years, ENSO variance increased rapidly to 30–40% higher than it is currently. Then, it was maintained at a relatively high level over the next 30 years (Fig. 8c). Such scenarios were accompanied by an increased frequency of ENSO events during 1852–1800 a BP (Fig. 8b). With the decline in ENSO frequency from 1800 a BP to 1780 a BP (Fig. 8b), ENSO variance dropped to 30–40% lower than the present level (Fig. 8c). Since 1780 a BP, ENSO variance has gradually risen to the modern level again, followed by a downward trend after 1760 a BP (Fig. 8c). The temporal transformation of ENSO variance coincides with the climatic shift reconstructed by Bainbridge sediment records, indicating that the remarkable increase in ENSO variability occurred in 1780 ± 230 a BP (Thompson et al., 2017). Additionally, a 20-year-long, annually resolved coral $\delta^{18}O$ time series recorded in fossil *Porites* microatolls from Christmas Island indicates that interannual variations in ENSO-related SST and precipitation were more pronounced at 1760 ± 85 a BP compared with modern standards (Woodroffe et al., 2003). McGregor and Gagan (2004) further estimated the amplitude of $\delta^{18}O$ anomalies recorded by Christmas Island *Porites* and found an extreme El Niño, nearly twice the amplitude of the 1997–1998 event. However, another fossil coral $\delta^{18}O$ record from Christmas Island demonstrates a 40% reduction in 2- to 7-year variance for 1704–1685 a BP compared with modern coral records for 1968–1998 CE (Cobb et al., 2013), which seemed in accordance with the descending trend of ENSO variance after 1760 a BP recorded by corals from the Xisha Islands.

Taken together, ENSO variability may have experienced a significant enhancement before 2010 a BP, an overall fluctuating attenuation from

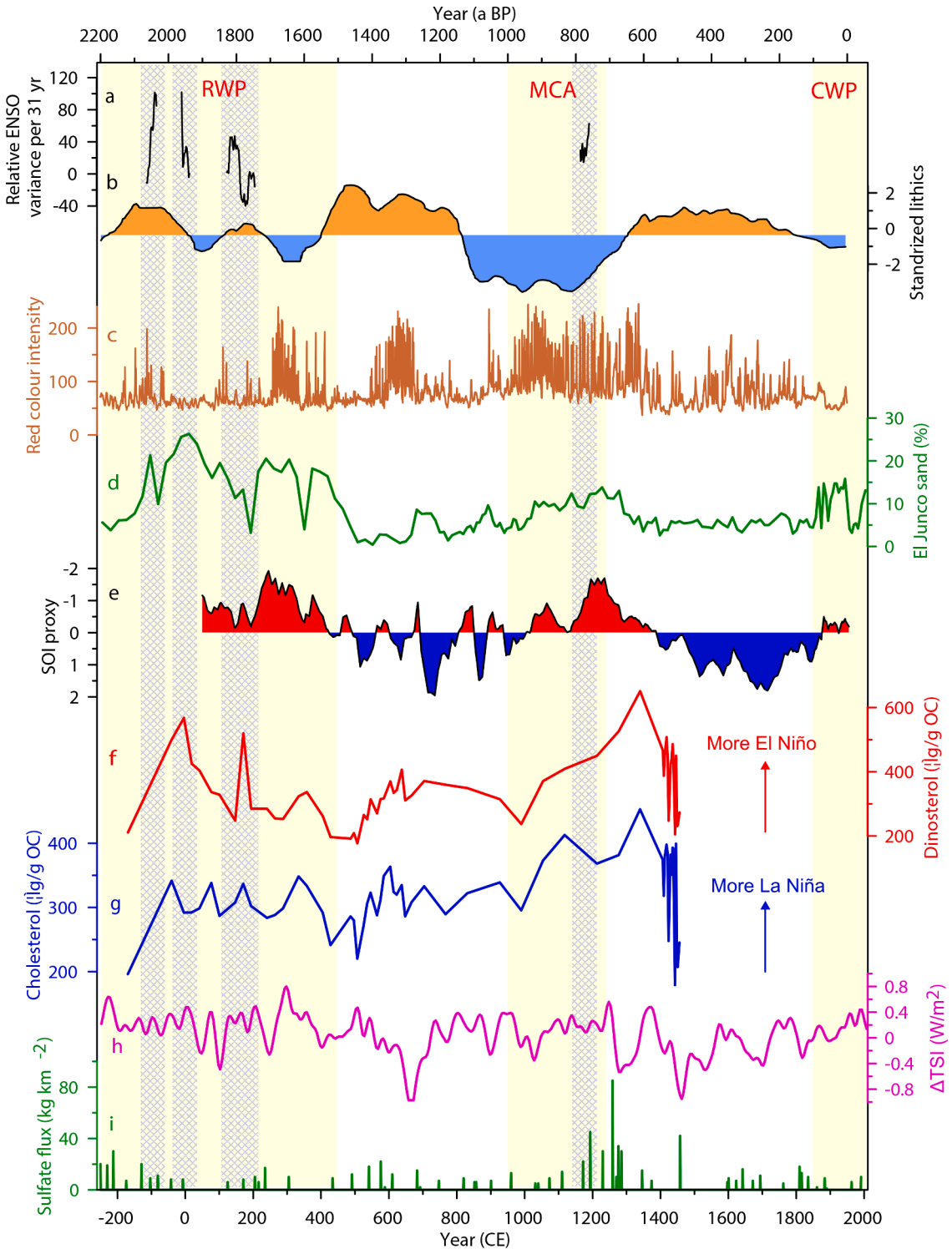

Fig. 9. Comparison of ENSO reconstructions with external forcings during the last 2000 years. (a) Relative ENSO variance for the filtered sub-fossil coral Sr/Ca-SST anomalies in a sliding 31-year window, plotted as percent differences from the intervals of modern coral (1980–2007 CE), during the Roman Warm Period (RWP) and Medieval Climate Anomaly (MCA; Jiang et al., 2021). (b) The standardized lithic concentration off the coast of Peru (Rein et al., 2005), modified from Sagawa et al. (2014). (c) Red colour intensity of sedimentation from Laguna Pallcacocha in southern Ecuador (Moy et al., 2002). (d) Percentage of sand in lake sediments from El Junco on the Galápagos Islands (Conroy et al., 2008). (e) Reconstructed Southern Oscillation Index-like records (Yan et al., 2011). (f) Dinosterol abundance from Peru (Makou et al., 2010). (g) Cholesterol abundance from Peru (Makou et al., 2010). (h) Variability of total solar irradiance (ΔTSI) based on the cosmogenic radionuclide ^{10}Be (Steinhilber et al., 2009). (i) Occurrence of major volcanic events through the last two millennium (Gautier et al., 2019). Gray and yellow vertical fields indicate the intervals in which sub-fossil corals lived and the warm periods, respectively. CWP, Current Warm Period. (For interpretation of the references to colour in this figure legend, the reader is referred to the web version of this article.)

1980 a BP to 1928 a BP, and two obvious processes of rising first before descending during 1852–1740 a BP (Fig. 9a). Although it was difficult to directly compare Xisha coral records with sedimentary ENSO records due to the obvious chronological uncertainty, ENSO variability within the RWP revealed by those sedimentary records was reliable and corroborated the results of this study. For example, sediments from Laguna Pallcacocha (Moy et al., 2002; Fig. 9c) and El Junco Crater Lake (Conroy et al., 2008; Fig. 9d) revealed that ENSO variability exhibits increments and reductions many times throughout the RWP. The numbers of El Niño (Fig. 9e-f) and La Niña events (Fig. 9g) show similar increasing and decreasing trends in this period (Makou et al., 2010; Yan et al., 2011). Combined with the intensified ENSO variability during the late MCA (Jiang et al., 2021; Fig. 9a), we considered that there has been a highly variable ENSO variability during the last 2000 years. Considering that the amplitude of orbital (Bertrand et al., 2002), total solar irradiance (Steinhilber et al., 2009; Fig. 9h), and major volcanic events (Gautier et al., 2019; Fig. 9i) during the RWP and the MCA was not only minimal but also similar to that preindustrial, the evolution of ENSO variability may be associated with internal dynamics of the climate system (Cobb et al., 2013; Wittenberg, 2009) or interdecadal modulation of ENSO variability (Li et al., 2011).

5.5. Seasonal pattern of interannual SST variability

Despite rising evidence for SST seasonality and interannual ENSO variability (Jiang et al., 2021; Liu et al., 2019; Wanamaker Jr. et al., 2011; Yan et al., 2017), few studies have investigated the relationship between them. Given that all coral Sr/Ca-SST seasonality showed prominent interannual variability (Fig. S6), it was considered that ENSO activity had a significant influence on SST seasonality in the northern SCS over the past 2000 years.

Observational results of instrumental SST have shown that ENSO activity predominantly affects the SST of the northern SCS in boreal winter through atmospheric teleconnections (Section 2). Spectral analysis of instrumental winter SST from the Xisha Islands depicts prominent interannual peaks centered at 2.4 and 7 years. Instrumental summer SST displayed similar variability at significant periodicities of 2.5 and 4.8 years (Fig. 7b). This mirrored the seasonal effect of ENSO activity on SST in the Xisha Islands. To shed light on the seasonal pattern of ENSO teleconnection for 2070–1740 a BP, monthly coral Sr/Ca-SST records were decomposed into seasonal time series and evaluated the interannual variations in different seasons. As shown in Fig. 7b, sub-fossil coral records demonstrate remarkable 2.5–4-year periodicities in summer and winter SSTs. This signifies that the seasonal pattern for the effects of ENSO on SST in the northern SCS existed 2000 years ago. For the RWP, ENSO activity was stronger with more frequent El Niño events approximately 1980 years ago. Under these circumstances, the anomalous anticyclone appeared in the northwestern Pacific, weakening the EAWM over the northern SCS. Therefore, winter SST in the Xisha Islands increased by ~0.6 °C, and SST seasonality decreased by ~1 °C correspondingly during 1980–1928 a BP.

In summary, the results suggest that interannual variability associated with ENSO activity plays a significant role in steering short-term changes in SST seasonality in the northern SCS. Considering that the frequency of extreme El Niño events may strengthen in the future under global warming (Cobb et al., 2013; Dee et al., 2020; Grothe et al., 2019), the climate around the northern SCS might grow more variable.

6. Conclusions

In this study, a combined 228-year-long, monthly coral Sr/Ca time series covering the period from 2070 a BP to 1740 a BP was developed using high-precision U-series-based chronologies from three *Porites* corals obtained from the Xisha Islands, northern SCS. While coral Sr/Ca-SST records provide additional evidence for the prevalence of cooler conditions in the western Pacific and East Asia during the RWP, the natural range of SST variations on seasonal and interannual timescales has also been investigated.

The comprehensive records reveal that SST seasonality during most of the RWP was similar to that in the present day, except for a lower value between 1980 a BP and 1928 a BP. Interannual variability associated with ENSO activity in 2070–1740 a BP was 39% stronger than that in 1980–2014 CE. However, the ENSO intensity in 1980–1928 a BP was obviously larger than that in 1852–1740 a BP, which was similar to the present results. The evolution of ENSO variability throughout the RWP was explored using an empirically calibrated threshold and sliding window. The reconstruction results demonstrate significantly enhanced ENSO variability during 2070–2010 a BP, followed by an overall fluctuating attenuation from 1980 a BP to 1928 a BP. Subsequently, ENSO variability has gone through the process of rising first before descending twice during 1852–1740 a BP. Furthermore, El Niño events play a dominant role in the evolution of ENSO variability, which may be associated with the internal dynamics of the climate system. Most importantly, prominent interannual variability found in all coral Sr/Ca-SST seasonalities reveals a significant role of ENSO variability in steering changes in SST seasonality in the northern SCS. This was primarily manifested in the decreased SST seasonality being usually accompanied by enhanced ENSO activity with more frequent El Niño events.

These findings provide unique insights into the natural range of SST variations in the northern SCS approximately 2000 years ago. However, additional high-resolution proxy reconstructions were necessary to fully characterize the range of ENSO variability and understand the mechanisms controlling the evolution of ENSO activity over the past two millennia.

Declaration of Competing Interest

The authors declare that they have no known competing financial interests or personal relationships that could have appeared to influence the work reported in this paper.

Acknowledgments

This work was supported by the National Science Foundation of China (Grant numbers 42030502 and 42090041), the Guangxi scientific projects (Grant numbers AD17129063 and AA17204074), and the Bagui Fellowship from Guangxi Province of China (Grant number 2014BGXZGX03). U-Th dating were carried out at the University of Queensland and was financially supported by an Australian Research Council discovery project (DP0773081). We acknowledge Gangjian Wei for providing the international coral standard (JCp-1 *Porites* spp.). We also appreciate Bojin Huang for her assistance with the sub-sampling. We sincerely appreciate the efforts of Editor Alan Haywood and two anonymous reviewers for their careful works and constructive suggestions, which greatly improved this manuscript.

Appendix A. Supplementary data

Supplementary data to this article can be found online at https://doi.org/10.1016/j.gloplacha.2021.103675.

References

Abram, N.J., McGregor, H.V., Gagan, M.K., Hantoro, W.S., Suwargadi, B.W., 2009. Oscillations in the southern extent of the Indo-Pacific warm Pool during the mid-Holocene. Quat. Sci. Rev. 28, 2794–2803. https://doi.org/10.1016/j.quascirev.2009.07.006.

Bertrand, C., Loutre, M.F., Crucifix, M., Berger, A., 2002. Climate of the last millennium: a sensitivity study. Paleoceanography 54A, 221–244. https://doi.org/10.1034/j.1600-0870.2002.00287.x.

Bjerknes, J., 1969. Atmospheric teleconnections from the equatorial pacific. Mon. Weather Rev. 97 (3), 163–172. https://doi.org/10.1175/1520-0493(1969)097<0163:ATFTEP>2.3.CO;2.

Box, G.E.P., Jenkins, G.M., Reinsel, G.C., 1976. Time Series Analysis: Forecasting and Control (Vol. 16). (Holden-Day San Francisco).
Büntgen, U., Tegel, W., Nicolussi, K., McCormick, M., Frank, D., Trouet, V., et al., 2011. 2500 years of European climate variability and human susceptibility. Science. https://doi.org/10.1126/science.1197175.
Chen, T., Cobb, K.M., Roff, G., Zhao, J., Yang, H., Hu, M., Zhao, K., 2018. Coral-derived western Pacific tropical sea surface temperatures during the last millennium. Geophys. Res. Lett. 45 (8), 3542–3549. https://doi.org/10.1002/2018gl077619.
Chu, K.C., 1973. Preliminary research on climate changes over the last 5000 years in China. Sci. Sinica 16 (2), 168–189.
Cobb, K.M., Charles, C.D., Cheng, H., Edwards, R.L., 2003. El Niño/Southern Oscillation and tropical Pacific climate during the last millennium. Nature 424 (6946), 271–276. https://doi.org/10.1038/nature01779.
Cobb, K.M., Westphal, N., Sayani, H.R., Watson, J.T., Lorenzo, E.D., Cheng, H., et al., 2013. Highly variable El Niño–Southern oscillation throughout the Holocene. Science 339 (6115), 67–70. https://doi.org/10.1126/science.1228246.
Cohen, A.L., Owens, K.E., Layne, G.D., Shimizu, N., 2002. The effect of algal symbionts on the accuracy of Sr/Ca paleotemperatures from coral. Science 296 (5566), 331–333. https://doi.org/10.1126/science.1069330.
Conroy, J.L., Restrepo, A., Overpeck, J.T., Kannan, M.S., Cole, J.E., Bush, M.B., et al., 2008. Unprecedented recent warming of surface temperatures in the eastern tropical Pacific Ocean. Nat. Geosci. 2 (1), 46–50. https://doi.org/10.1038/NGEO390.
Corrège, T., 2006. Sea surface temperature and salinity reconstruction from coral geochemical tracers. Palaeogeogr. Palaeoclimatol. Palaeoecol. 232 (2–4), 408–428. https://doi.org/10.1016/j.palaeo.2005.10.014.
D'Arrigo, R., Cook, E.R., Wilson, R.J., Allan, R., Mann, M.E., 2005. On the variability of ENSO over the past six centuries. Geophys. Res. Lett. 32, L03711 https://doi.org/10.1029/2004GL022055.
de Villiers, S., Nelson, B.K., Chivas, A.R., 1995. Biological controls on coral Sr/Ca and $\delta^{18}O$ reconstructions of sea surface temperatures. Science 269, 1247–1249.
Dee, S.G., Cobb, K.M., Emile-Geay, J., Ault, T.R., Edwards, R.L., Cheng, H., Charles, C.D., 2020. No consistent ENSO response to volcanic forcing over the last millennium. Science 367 (6485), 1477–1481. https://doi.org/10.1126/science.aax2000.
DeLong, K.L., Flannery, J.A., Maupin, C.R., Poore, R.Z., Quinn, T.M., 2011. A coral Sr/Ca calibration and replication study of two massive corals from the Gulf of Mexico. Palaeogeogr. Palaeoclimatol. Palaeoecol. 307 (1–4), 117–128. https://doi.org/10.1016/j.palaeo.2011.05.005.
DeLong, K.L., Quinn, T.M., Taylor, F.W., Shen, C.C., Lin, K., 2013. Improving coral- base paleoclimate reconstructions by replicating 350 years of coral Sr/Ca variations. Palaeogeogr. Palaeoclimatol. Palaeoecol. 373, 6–24. https://doi.org/10.1016/j.palaeo.2012.08.019.
DeLong, K.L., Flannery, J.A., Poore, R.Z., Quinn, T.M., Maupin, C.R., Lin, K., Shen, C.-C., 2014. A reconstruction of sea surface temperature variability in the southeastern Gulf of Mexico from 1734 to 2008 C.E. using cross-dated Sr/Ca records from the coral *Siderastrea siderea*. Paleoceanography 29, 403–422. https://doi.org/10.1002/2013PA002524.
Deng, W., Wei, G., Zhao, J.X., Zeng, T., 2019. Anthropogenic effects on tropical oceanic climate change and variability: an insight from the South China Sea over the past 2000 years. Quat. Sci. Rev. 206, 56–64. https://doi.org/10.1016/j.quascirev.2018.12.027.
Denton, G.H., Alley, R.B., Comer, G.C., Broecker, W.S., 2005. The role of seasonality in abrupt climate change. Quat. Sci. Rev. 24 (10), 1159–1182. https://doi.org/10.1016/j.quascirev.2004.12.002.
Deser, C., Alexander, M.A., Xie, S.-P., Phillips, A.S., 2010. Sea surface temperature variability: patterns and mechanisms. Annu. Rev. Mar. Sci. 2 (1), 115–143. https://doi.org/10.1146/annurev-marine-120408-151453.
Felis, T., Lohmann, G., Kuhnert, H., Lorenz, S.J., Scholz, D., Pätzold, J., Al-Rousan, S.A., Al-Moghrabi, S.M., 2004. Increased seasonality in Middle East temperatures during the last interglacial period. Nature 429 (6988), 164–168. https://doi.org/10.1038/nature02546.
Gagan, M.K., Ayliffe, L.K., Hopley, D., Cali, J.A., Mortimer, G.E., Chappell, J., McCulloch, M.T., et al., 1998. Temperature and surface-ocean water balance of the Mid-Holocene tropical western Pacific. Science 279 (5353), 1014–1018. https://doi.org/10.1126/science.279.5353.1014.
Gautier, E., Savarino, J., Hoek, J., Erbland, J., Caillon, N., Hattori, S., et al., 2019. 2600-years of stratospheric volcanism through sulfate isotopes. Nat. Commun. 10 (1) https://doi.org/10.1038/s41467-019-08357-0.
Ge, Q.S., Zheng, J.Y., Hao, Z.X., Liu, H.L., 2013. General characteristics of climate changes during the past 2000 years in China. Sci. China Earth Sci. 56, 321–329. https://doi.org/10.1007/s11430-012-4370-y.
Ghil, M., Allen, M.R., Dettinger, M.D., Ide, K., Kondrashov, D., Mann, M.E., et al., 2002. Advanced spectral methods for climatic time series. Rev. Geophys. 40 (1) https://doi.org/10.1029/2000RG000092.
Giry, C., Felis, T., Kling, M., Scholz, D., Wei, W., Lohmann, G., et al., 2012. Mid- to late Holocene changes in tropical Atlantic temperature seasonality and interannual to multidecadal variability documented in southern Caribbean corals. Earth Planet. Sci. Lett. 331–332, 187–200. https://doi.org/10.1016/j.epsl.2012.03.019.
Grothe, P.R., Cobb, K.M., Liguori, G., Lorenzo, E.D., Capotondi, A., Lu, Y., et al., 2019. Enhanced El Niño-Southern Oscillation variability in recent decades. Geophys. Res. Lett. 47 (7) https://doi.org/10.1029/2019GL083906.
Hathorne, E.C., Gagnon, A., Felis, T., Adkins, J., Asami, R., Boer, W., et al., 2013. Interlaboratory study for coral Sr/Ca and other element/Ca ratio measurements. Geochem. Geophys. Geosyst. 14 (9), 3730–3750. https://doi.org/10.1002/ggge.20230.
Huang, B., Yu, K., Zhang, H., Shi, Q., Chen, T., Tao, S., et al., 2013. Sea surface temperature variations during the middle Rome warm period as reconstructed by *Porites* coral growth rates in the Xisha Islands. Trop. Geogr. 33 (3), 237–241 (In Chinese with English abstract).
Jiang, L., Yu, K., Tao, S., Wang, S., Han, T., Jiang, W., 2021. ENSO variability during the medieval climate Anomaly as recorded by *Porites* corals from the northern South China Sea. Paleoceanogr. Paleoclimatol. https://doi.org/10.1029/2020PA004173.
Klein, S.A., Soden, B.J., Lau, N., 1999. Remote Sea surface temperature variations during ENSO: evidence for a tropical atmospheric bridge. J. Clim. 12 (4), 917–932.
Kong, D., Wei, G., Chen, M., Peng, S., Liu, Z., 2017. Northern South China Sea SST changes over the last two millennia and possible linkage with solar irradiance. Quat. Int. 459, 29–34. https://doi.org/10.1016/j.quaint.2017.10.001.
Koutavas, A., DeMenocal, P.B., Olive, G.C., Lynch-Stieglitz, J., 2006. Mid-Holocene El Niño-Southern Oscillation attenuation revealed by individual foraminifera in eastern tropical Pacific sediments. Geology 34 (12), 993–996. https://doi.org/10.1130/G22810A.1.
Lamb, H.H., 1977. Climate: Present, Past and Future–V.2: Climatic History and the Future (Methuen, London), p. 837.
Lawman, A.E., Quinn, T.M., Partin, J.W., Thirumalai, K., Taylor, F.W., Wu, C.-C., et al., 2020. A century of reduced ENSO variability during the Medieval Climate Anomaly. Paleoceanogr. Paleoclimatol. 35 https://doi.org/10.1029/2019PA003742 e2019PA003742.
Li, C., 1990. Interaction between anomalous winter monsoon in East Asia and El Niño event. Adv. Atmos. Sci. 7, 36–46.
Li, J.B., Xie, S.P., Cook, E.R., Huang, G., D'Arrigo, R., Liu, F., et al., 2011. Interdecadal modulation of El Niño amplitude during the past millennium. Nat. Clim. Chang. 1 (2), 114–118. https://doi.org/10.1038/NCLIMATE1086.
Linsley, B.K., Wellington, G.M., Schrag, D.P., 2000. Decadal Sea surface temperature variability in the subtropical South Pacific from 1726 to 1997 A.D. Science 290 (5494), 1145–1148. https://doi.org/10.1126/science.290.5494.1145.
Linsley, B.K., Kaplan, A., Gouriou, Y., Salinger, J., de Menocal, P.B., Wellington, G.M., Howe, S.S., 2006. Tracking the extent of the South Pacific Convergence Zone since the early 1600s. Geochem. Geophys. Geosyst. 7 (5) https://doi.org/10.1029/2005gc001115 n/a–n/a.
Liu, C., Yan, H., Fei, H., Ma, X., Zhang, W., Shi, G., et al., 2019. Temperature seasonality and ENSO variability in the northern South China Sea during the medieval climate anomaly interval derived from the Sr/Ca ratios of *Tridacna* shell. J. Asian Earth Sci. 180 (103880), 1–9. https://doi.org/10.1016/j.jseaes.2019.103880.
Ljungqvist, F.C., 2010. A new reconstruction of temperature variability in the extra-tropical Northern Hemisphere during the last two millennia. Geogr. Ann. 92 (3), 339–351. https://doi.org/10.1111/j.1468-0459.2010.00399.x.
Makou, M.C., Eglinton, T.I., Oppo, D.W., Hughen, K.A., 2010. Postglacial changes in El Niño and La Niña behavior. Geology 38 (1), 43–46. https://doi.org/10.1130/g30366.1.
Martín-Puertas, C., Valero-Garcés, B.L., Brauer, A., Mata, M.P., Delgado-Huertas, A., Dulski, P., 2009. The Iberian–Roman Humid Period (2600–1600 cal yr BP) in the Zoñar Lake varve record (Andalucía, southern Spain). Quat. Res. 71, 108–120. https://doi.org/10.1016/j.yqres.2008.10.004.
McGregor, H.V., Gagan, M.K., 2004. Western Pacific coral $\delta^{18}O$ records of anomalous Holocene variability in the El Niño-Southern Oscillation. Geophys. Res. Lett. 31 (11), L11204 https://doi.org/10.1029/2004GL019972.
McGregor, H.V., Fischer, M.J., Gagan, M.K., Fink, D., Phipps, S.J., Wong, H., Woodroffe, C.D., 2013. A weak El Niño/Southern Oscillation with delayed seasonal growth around 4,300 years ago. Nat. Geosci. 6 (11), 949–953. https://doi.org/10.1038/NGEO1936.
Mitsuguchi, T., Dang, P.X., Kitagawa, H., Uchida, T., Shibata, Y., 2008. Coral Sr/Ca and Mg/Ca records in con Dao Island off the Mekong Delta: Assessment of their potential for monitoring ENSO and East Asian monsoon. Glob. Planet. Chang. 63, 341–352. https://doi.org/10.1016/j.gloplacha.2008.08.002.
Moberg, A., Sonechkin, D.M., Holmgren, K., Datsenko, N.M., Karlén, W., 2005. Highly variable northern hemisphere temperatures reconstructed from low- and high-resolution proxy data. Nature 433 (7026), 613–617. https://doi.org/10.1038/nature03265.
Moy, C.M., Seltzer, G.O., Rodbell, D.T., Anderson, D.M., 2002. Variability of El Niño/Southern Oscillation activity at millennial timescales during the Holocene epoch. Nature 420 (6912), 162–165. https://doi.org/10.1038/nature01194.
Neukom, R., Steiger, N., Gómez-Navarro, J.J., Wang, J., Werner, J.P., 2019. No evidence for globally coherent warm and cold periods over the preindustrial Common Era. Nature 571, 550–553. https://doi.org/10.1038/s41586-019-1401-2.
Okai, T., Suzuki, A., Kawahata, H., Terashima, S., Imai, N., 2002. Preparation of a new geological survey of Japan geochemical reference material: Coral JCp-1. Geostand. Newslett. 26 (1), 95–99. https://doi.org/10.1111/j.1751-908X.2002.tb00627.x.
Oppo, D.W., Rosenthal, Y., Linsley, B.K., 2009. 2000-year-long temperature and hydrology reconstructions from the Indo-Pacific warm pool. Nature 460 (7259), 1113–1116. https://doi.org/10.1038/nature08233.
Patterson, W.P., Dietrich, K.A., Holmden, C., Andrews, J.T., 2010. Two millennia of North Atlantic seasonality and implications for Norse colonies. Proc. Natl. Acad. Sci. 107 (12), 5306–5310. https://doi.org/10.1073/pnas.0902522107.
Rayner, N.A., Parker, D.E., Horton, E.B., Folland, C.K., Alexander, L.V., Rowell, D.P., et al., 2003. Global analyses of sea surface temperature, sea ice, and night marine air temperature since the late nineteenth century. J. Geophys. Res. 108 (14), 4407. https://doi.org/10.1029/2002JD002670.
Rein, B., Luckge, A., Reinhardt, L., Sirocko, F., Wolf, A., Dullo, W.C., 2005. El Niño variability off Peru during the last 20,000 years. Paleoceanography 20 (4), PA4003. https://doi.org/10.1029/2004PA001099.
Reynolds, R.W., Rayner, N.A., Smith, T.M., Stokes, D.C., Wang, W., 2002. An improved in situ and satellite SST analysis for climate. J. Clim. 15 (13), 1609–1625. https://doi.org/10.1175/1520-0442(2002)015<1609.

Riedinger, M.A., Steinitz-Kannan, M., Last, W.M., Brenner, M., 2002. A 6100 ^{14}C yr record of El Niño activity from the Galápagos Islands. J. Paleolimnol. 27 (1), 1–7. https://doi.org/10.1023/A:1013514408468.

Sagawa, T., Kuwae, M., Tsuruoka, K., Nakamura, Y., Ikehara, M., Murayama, M., 2014. Solar forcing of centennial-scale East Asian winter monsoon variability in the mid- to late Holocene. Earth Planet. Sci. Lett. 395, 124–135. https://doi.org/10.1016/j.epsl.2014.03.043.

Sayani, H.R., Cobb, K.M., Delong, K., Hitt, N.T., Druffel, E.R.M., 2019. Inter-colony δ^{18}O and Sr/Ca variability among *Porites* spp. corals at Palmyra Atoll: toward more robust coral-based estimates of climate. Geochem. Geophys. Geosyst. 20 (11), 5270–5284. https://doi.org/10.1029/2019GC008420.

Schrag, D.P., 1999. Rapid analysis of high-precision Sr/Ca ratios in corals and other marine carbonated. Paleoceanography 14 (2), 97–102. https://doi.org/10.1029/1998PA900025.

Smith, T.M., Reynolds, R.W., Peterson, T.C., Lawrimore, J., 2008. Improvements to NOAA's historical merged land–ocean surface temperature analysis (1880–2006). J. Clim. 21 (10), 2283–2296. https://doi.org/10.1175/2007JCLI2100.1.

Steinhilber, F., Beer, J., Frhlich, C., 2009. Total solar irradiance during the Holocene. Geophys. Res. Lett. 36 (19) https://doi.org/10.1029/2009GL040142.

Steinke, S., Prange, M., Feist, C., Groeneveld, J., Mohtadi, M., 2014. Upwelling variability off southern Indonesia over the past two millennia. Geophys. Res. Lett. 41, 7684–7693. https://doi.org/10.1002/2014GL061450.

Stott, L., Cannariato, K., Thunell, R., Haug, G.H., Koutavas, A., Lund, S., 2004. Decline of surface temperature and salinity in the western tropical pacific ocean in the Holocene epoch. Nature 431 (7004), 56–59. https://doi.org/10.1038/nature02903.

Su, Y., Fang, X.Q., Yin, J., 2014. Impact of climate change on fluctuations of grain harvests in China from the Western Han Dynasty to the five Dynasties (206 BC–960 AD). Sci. China Earth Sci. 57, 1701–1712. https://doi.org/10.1007/s11430-013-4795-y.

Surge, D., Barrett, J.H., 2012. Marine climatic seasonality during medieval times (10th to 12th centuries) based on isotopic records in Viking Age shells from Orkney, Scotland. Palaeogeogr. Palaeoclimatol. Palaeoecol. 350–352, 236–246. https://doi.org/10.1016/j.palaeo.2012.07.003.

Tan, M., Liu, T., Hou, J., Qin, X., Zhang, H., Li, T., 2003. Cyclic rapid warming on centennial-scale revealed by a 2650-year stalagmite record of warm season temperature. Geophys. Res. Lett. 30 (12) https://doi.org/10.1029/2003GL017352.

Thompson, D.M., Conroy, J.L., Collins, A., Hlohowskyj, S.R., Overpeck, J.T., Whitmore, M.R., et al., 2017. Tropical Pacific climate variability over the last 6000 years as recorded in Bainbridge Crater Lake, Galápagos. Paleoceanography 32, 903–922. https://doi.org/10.1002/2017PA003089.

Timmermann, A., An, S., Kug, J., Jin, F., Cai, W., Capotondi, A., et al., 2018. El Niño–Southern oscillation complexity. Nature 559 (7715), 535–545. https://doi.org/10.1038/s41586-018-0252-6.

Wanamaker Jr., A.D., Kreutz, K.J., Schöne, B.R., Introne, D.S., 2011. Gulf of Maine shells reveal changes in seawater temperature seasonality during the medieval climate Anomaly and the Little Ice Age. Palaeogeogr. Palaeoclimatol. Palaeoecol. 302 (1), 43–51. https://doi.org/10.1016/j.palaeo.2010.06.005.

Wang, B., Wu, R., Fu, X., 2000. Pacific–East Asian teleconnection: how does ENSO affect East Asian climate? J. Clim. 13 (9), 1517–1536. https://doi.org/10.1175/1520-0442(2000)013<1517:PEATHD>2.0.CO;2.

Wang, T., Surge, D., Mithen, S., 2012. Seasonal temperature variability of the Neoglacial (3300–2500 BP) and Roman Warm Period (2500–1600 BP) reconstructed from oxygen isotope ratios of limpet shells (*Patella vulgata*), Northwest Scotland. Palaeogeogr. Palaeoclimatol. Palaeoecol. 317–318, 104–113. https://doi.org/10.1016/j.palaeo.2011.12.016.

Wang, X., Deng, W., Liu, X., Wei, G., Chen, X., Zhao, J., et al., 2018. Super instrumental El Niño events recorded by a *Porites* coral from the South China Sea. Coral Reefs 37 (1), 295–308. https://doi.org/10.1007/s00338-018-1658-1.

Wang, L.-C., Tang, Z.-W., Chen, H.-F., Li, H.-C., Shiau, L.-J., Huang, J.-J.S., et al., 2019. Late Holocene vegetation, climate, and natural disturbance records from an alpine pond in Central Taiwan. Quat. Int. 528, 63–72. https://doi.org/10.1016/j.quaint.2019.03.005.

Wittenberg, A.T., 2009. Are historical records sufficient to constrain ENSO simulations? Geophys. Res. Lett. 36, L12702 https://doi.org/10.1029/2009GL038710.

Woodroffe, C.D., Beech, M.R., Gagan, M.K., 2003. Mid-late Holocene El Niño variability in the equatorial Pacific from coral microatolls. Geophys. Res. Lett. 30 (7), 1358. https://doi.org/10.1029/2002GL015868.

Wu, W., Tan, W., Zhou, L., Yang, H., Xu, Y., 2012. Sea surface temperature variability in southern Okinawa Trough during last 2700 years. Geophys. Res. Lett. 39 (14), 36–57. https://doi.org/10.1029/2012GL052749.

Wyrtki, K., 1961. Physical Oceanography of the Southeast Asian Waters: Scientific Results of Marine Investigations of the South China Sea and the Gulf of Thailand 1959–1961. *Naga Report*, 2. Scripps Institution of Oceanography, USA (https://doi.org/repositories.cdlib.org/sio/naga/2).

Yan, H., Sun, L., Wang, Y., Huang, W., Qiu, S., Yang, C., 2011. A record of the Southern Oscillation Index for the past 2,000 years from precipitation proxies. Nat. Geosci. 4 (9), 611–614. https://doi.org/10.1038/ngeo1231.

Yan, H., Soon, W., Wang, Y., 2015a. A composite sea surface temperature record of the northern South China Sea for the past 2500 years: a unique look into seasonality and seasonal climate changes during warm and cold periods. Earth Sci. Rev. 141, 122–135. https://doi.org/10.1016/j.earscirev.2014.12.003.

Yan, H., Sun, L., Shao, D., Wang, Y., 2015b. Seawater temperature seasonality in the South China Sea during the late Holocene derived from high-resolution Sr/Ca ratios of *Tridacna gigas*. Quat. Res. 83 (2), 298–306. https://doi.org/10.1016/j.yqres.2014.12.001.

Yan, H., Liu, C., Zhang, W., Li, M., Zheng, X., Wei, G., et al., 2017. ENSO variability around 2000 years ago recorded by *Tridacna* gigas δ^{18}O from the South China Sea. Quat. Int. 452, 148–154. https://doi.org/10.1016/j.quaint.2016.05.011.

Yu, K.F., 2012. Coral reefs in the South China Sea: their response to and records on past environmental changes. Sci. China Earth Sci. 42 (8), 1160–1172. https://doi.org/10.1007/s11430-012-4449-5.

Yu, K.F., Zhao, J.X., Wei, G.J., Cheng, X.R., Chen, T.G., Felis, T., et al., 2005a. δ^{18}O, Sr/Ca and Mg/Ca records of *Porites lutea* corals from Leizhou Peninsula, northern South China Sea, and their applicability as paleoclimatic indicators. Palaeogeogr. Palaeoclimatol. Palaeoecol. 218 (1–2), 57–73. https://doi.org/10.1016/j.palaeo.2004.12.003.

Yu, K.F., Zhao, J.X., Wei, G.J., Cheng, X.R., Wang, P.X., 2005b. Mid-late Holocene monsoon climate retrieved from seasonal Sr/Ca and δ^{18}O records of *Porites lutea* corals at Leizhou Peninsula, northern coast of South China Sea. Glob. Planet. Chang. 47 (2–4), 301–316. https://doi.org/10.1016/j.gloplacha.2004.10.018.

Yu, K.F., Zhao, J., Shi, Q., Chen, T., Wang, P., Collerson, K.D., Liu, T., 2006. U-series dating of dead *Porites* corals in the South China Sea: evidence for episodic coral mortality over the past two centuries. Quat. Geochronol. 1 (2), 129–141. https://doi.org/10.1016/j.quageo.2006.06.005.

Yu, K.F., Zhao, J.X., Shi, Q., Price, G.J., 2012. Recent massive coral mortality events in the South China Sea: was global warming and ENSO variability responsible? Chem. Geol. 320–321, 54–65. https://doi.org/10.1016/j.chemgeo.2012.05.028.